Elastic electron scattering on exotic light proton-rich nuclei

Zaijun Wang[1,*] and Zhongzhou Ren[1,2]
[1]*Department of Physics, Nanjing University, Nanjing 210008, China*
[2]*Center of Theoretical Nuclear Physics, National Laboratory of Heavy-Ion Accelerator at Lanzhou, Lanzhou 730000, China*
(Received 29 April 2004; published 10 September 2004)

Recent experiments show that there may exist proton halos in exotic light proton-rich nuclei. We investigate the effect of an extended proton density distribution on the cross sections and form factors of elastic electron scattering from the exotic proton drip-line nuclei ^{28}S and ^{12}O. With charge density distributions from the self-consistent relativistic mean field model, we calculate the cross sections and form factors for elastic electron scattering in the eikonal approximation. The numerical results are compared with the available data of the stable nuclei ^{32}S and ^{16}O. The results show that the form factors and cross sections for elastic electron scattering at intermediate-momentum transfers are very sensitive to the alterations of the charge density distributions of the last protons in exotic nuclei ^{28}S and ^{12}O. This is an interesting combination of the reliable relativistic mean field model with the model of electron-nucleus scattering and it can be useful for future experiments.

DOI: 10.1103/PhysRevC.70.034303 PACS number(s): 25.30.Bf, 21.10.Ft, 27.30.+t, 13.40.Gp

I. INTRODUCTION

Nuclear halo is a well-known phenomenon in nuclear physics. Tanihata *et al.* found that the neutron-rich nucleus ^{11}Li had an abnormally large matter root-mean-square radius [1,2]. Further experiments confirmed that there are neutron halos in other neutron-rich nuclei such as ^{6,8}He, ^{11,14}Be, ^{17}B, and ^{19}C [3–5]. Neutron halos manifest themselves as extended neutron density distributions in exotic neutron-rich nuclei. The cause of occurrence of the halo phenomenon lies in both the small separation energy of the last few nucleons and their occupation on the orbits with low angular momentum. Many experiments [6–9] have been performed to study neutron halos in neutron-rich nuclei and neutron-halo nuclei are well identified in light mass region. Theoretically neutron halos in exotic nuclei ^{6,8}He, ^{11}Li, ^{11,14}Be, ^{17}B, and ^{19}C have also been well reproduced by various theoretical models [10–15].

Although neutron halos have been well investigated in neutron-rich nuclei, studies on proton halos are relatively less. Theoretically, much effort has been made to the search of proton halos in proton drip-line nuclei. Calculations show that there may be proton halos in ^{26,27,28}P [16,17], ^{8}B, ^{17}Ne, and the excited state of ^{6}Li and ^{17}F. Experiments also show some indications of the existence of proton halos in these nuclei [18–23]. However, further experiments are needed to confirm the existence of the proton halos. Thus, the proton halo phenomenon is a very interesting subject of investigation.

The present experimental methods to identify the neutron halos and proton ones are mainly based on the measurement of the reaction cross sections of the nucleus-nucleus collision and of the momentum distributions of nucleus breakup. There are complex processes where the strong and electromagnetic interactions among nucleons play a role. Although this class of experiments has reached primary success for halo phenomena, it is interesting to search for a new probe to refine the study of charged halos. Electron-nucleus scattering has proven to be an excellent tool for the study of nuclear structure, especially for the research of electromagnetic properties of nuclei. It has provided much reliable information on charge density distributions of stable nuclei. Thus, we consider that the electron-nucleus scattering is a better way for the precise investigation of the extended charge distribution of the exotic proton-rich nuclei. Unfortunately the electron scattering on exotic nuclei was not possible in the past because of the difficulty of making targets from unstable nuclei. Recently a new collider of electron and unstable nucleus is under construction at RIKEN in Japan [24]. A similar collider at GSI in Germany [25] was also approved by the German government and will be built immediately. So the scattering of electron from unstable nuclei will be available soon. These new facilities will provide a good opportunity to study the charge density distributions of unstable nuclei by elastic electron scattering. Therefore, it is interesting to make an exploratory investigation of elastic electron scattering from proton-rich nuclei.

In the traditional model of electron scattering from nuclei, the charge density distribution of the target is usually replaced with some simple charge density models, such as the 3PF model or the harmonic oscillator model, or obtained by the phenomenological harmonic potential or Woods-Saxon potential. The scattering cross sections and form factors are calculated based on the outputs of these phenomenological potentials. Although these potentials work well for stable nuclei, their reliability for unstable nuclei is unknown. In order to study the elastic electron scattering from unstable nuclei, we need to find a more reliable model to produce the charge density distributions for the exotic nuclei out to the proton and neutron drip lines. Very recently the self-consistent relativistic mean field (RMF) model has been widely applied to both the stable nuclei and the unstable nuclei [26–29]. A series of calculations show that the RMF model can reproduce with good precision the binding energies, the separation

*Electronic address: zaijunwang99@hotmail.com

energies, and the radii of charge density distributions. The experimental isotope shifts of charge radii on some isotopic chains are also reproduced by the model [30]. Therefore, it is interesting to combine this successful nuclear structure model with the model of electron scattering for a reliable prediction of the cross sections and form factors of exotic proton-rich nuclei.

In this paper we choose the light nuclei ^{12,16}O and ^{28,32}S as the candidates to see the effect of the extended charge distribution on the process of elastic electron scattering. ^{16}O and ^{32}S are two reference nuclei where experimental data (differential cross sections) are available [31,32]. The nuclei ^{12}O and ^{28}S are two typical proton drip-line nuclei where their proton density distributions have an extended tail as compared with those of the stable nuclei. So the nuclei ^{12}O and ^{28}S should be considered as the model nuclei for theoretical calculations. It is expected that the conclusions drawn from them will be valid for other light proton drip-line nuclei.

This paper is organized in the following way. Section II is the formalism of elastic electron scattering and the simple description of the RMF model. The numerical results and discussions are presented in Sec. III. A summary is given in Sec. IV.

II. FORMALISM

A. The eikonal approximation

Because we study elastic electron scattering on light nuclei ^{32,28}S and ^{16,12}O at high energies in the present paper, we use the eikonal approximation [33–37] as a starting point for our calculations. The eikonal approximation can be sufficiently accurate and the underlying physics in it is much transparent. Hence, we use it to look for the features of elastic electron scattering on light unstable nuclei. Expressions of the eikonal approximation for ultrarelativistic electron scattering from a charge distribution can be found in Refs. [36] and [37]. Here we just review the essentials. The elastic differential cross section σ and form factor $F(q)$ in the eikonal approximation can be expressed as [36]

$$\sigma = \cos^2\left(\tfrac{1}{2}\theta\right)|I_1(q) + I_2(q)|^2, \tag{1}$$

and

$$|F(q)|^2 = \frac{\sigma}{\sigma_M}, \tag{2}$$

where θ is the scattering angle, q is the momentum transfer, σ_M is the Mott cross section, and $I_1(q)+I_2(q)$ is the scattering amplitude. $I_1(q)$ and $I_2(q)$ are given by the following integrals:

$$I_1(q) = -ik\int_0^R J_0(qb)[e^{2i\chi(b)} - 1]b\, db, \tag{3}$$

$$I_2(q) = -ik\int_R^\infty J_0(qb)[e^{2i\chi(b)} - 1]b\, db, \tag{4}$$

where b is the impact parameter, R is the cutoff cylindrical radius, $k=|\mathbf{k}|$, $\mathbf{k}$ is the three momentum of the incident electrons, and J_0 is the Bessel function. For high energy electrons ($E \simeq k$), $\chi(b)$ can be written as [36,37]:

$$\chi(b) = -\frac{1}{2}\int_{-\infty}^{\infty} V(r)dz, \tag{5}$$

$$r = \sqrt{b^2 + z^2}. \tag{6}$$

Since the charge density vanishes beyond R, $V(r)$ can be replaced by the Coulomb potential in this region.

For the region $b > R$, it is evident that Eq. (5) is divergent logarithmically for the Coulomb potential. To cope with this difficulty, we use Glauber's method [37]. The main point consists in screening the Coulomb potential, which is subsequently moved to an arbitrarily large distance from the scattering center. According to Glauber's method the screened Coulomb potential for electrons can be written in the form

$$V(r) = -\frac{Z\alpha}{r}H(r), \tag{7}$$

where $H(r)$ vanishes as r tends to infinity. The screening function $H(r)$ can be chosen as a step function [37]:

$$H(r) = \begin{cases} 1, & r \leqslant a \\ 0, & r > a, \end{cases} \tag{8}$$

where a is the screening distance. When $V(r)$ is replaced by Eq. (7), the integral in Eq. (5) can be done analytically. The result is [36,37]:

$$\chi(b) = \begin{cases} \alpha Z \ln\left[\dfrac{a + (a^2 - b^2)^{1/2}}{b}\right], & b \leqslant a \\ 0, & b > a. \end{cases} \tag{9}$$

For large screening distance $a(b/a \ll 1)$, $\chi(b)$ can be expanded in powers of b/a,

$$\chi(b) = -\alpha Z \ln\left(\frac{b}{2a}\right) + O\left(\frac{b^2}{a^2}\right). \tag{10}$$

As shown in Ref. [36], $\chi(b)$ can also be expressed as a function of cutoff radius R:

$$\chi(b) = -\alpha Z \ln\left(\frac{b}{R}\right). \tag{11}$$

Upon substituting Eq. (11) into Eq. (4) and carrying out the integral (details can be found in the Appendix of Ref. [36]), Eq. (4) becomes

$$I_2(q) = i\frac{k}{q^2}[-i2\alpha Z(qR)^{i2\alpha Z+1}J_0(qR)S_{-i2\alpha Z,-1}(qR) \tag{12}$$

$$+ (qR)^{i2\alpha Z+1}J_1(qR)S_{1-i2\alpha Z,0}(qR) - (qR)J_1(qR)], \tag{13}$$

where $S_{\mu\nu}(Z)$ are Lommel's functions and J_0 and J_1 are Bessel functions. For large $R(R \geqslant 8$ fm), the following asymptotic expansion of Lommel's functions can be used:

$$S_{\mu\nu}(Z) \simeq Z^{\mu-1}\left[1-\frac{(\mu-1)^2-\nu^2}{Z^2}+\frac{((\mu-1)^2-\nu^2)((\mu-3)^2-\nu^2)}{Z^4}-\ldots\right]. \quad (14)$$

For the region $b<R$, $\chi(b)$ is given by [36]:

$$\chi(b) = -Z\alpha \log\left(\frac{b}{R}\right) - 4\pi\alpha\int_b^R r^2\rho(r)y\left(\frac{b}{r}\right)dr, \quad (15)$$

where

$$y(x) = \log\left[\frac{1+(1-x^2)^{\frac{1}{2}}}{x}\right] - (1-x^2)^{1/2}, \quad (16)$$

and $\rho(r)$ is the charge density distribution, which satisfies the following normalization relation:

$$\int \rho(r)d\mathbf{r} = Z. \quad (17)$$

Since we are concentrating on high-energy electron scattering on light nuclei with proton number $Z\leqslant 20$, the recoil effect must be taken into account. We take into account the recoil of the target nucleus by dividing the cross section by the factor [32]:

$$f_{\rm rec} = \left(1+\frac{2E\sin^2\frac{\theta}{2}}{Mc^2}\right), \quad (18)$$

where E is the incident energy. Another correction to our calculation is the Coulomb attraction felt by the electrons. We take it into account with the standard method in electron scattering on light nuclei. That is to replace the momentum transfer q with the effective momentum transfer

$$q_{\rm eff} = q[1+1.5\alpha Z\hbar c/(ER_0)], \quad (19)$$

in our calculation, where $R_0=1.07A^{1/3}$, A is the mass number of the nucleus.

The earlier Eqs. (1)–(17) along with the corrections (18) and (19) enable us to calculate the elastic scattering cross sections and form factors for a given charge density distribution.

B. The relativistic mean-field model

Since the RMF model is a standard theory and the details can be found in many works [26–29], we only give the main elements here. The starting point of this model is an effective Lagrange density $\mathcal{L}$ for the interacting nucleons, the σ, ω, ρ mesons, and photons

$$\begin{aligned}\mathcal{L} = {}& \bar{\Psi}(i\gamma^\mu\partial_\mu - m)\Psi - g_\sigma\bar{\Psi}\sigma\Psi - g_\omega\bar{\Psi}\gamma^\mu\omega_\mu\Psi \\ & - g_\rho\bar{\Psi}\gamma^\mu\rho_\mu^a\tau^a\Psi + \tfrac{1}{2}\partial^\mu\sigma\partial_\mu\sigma - \tfrac{1}{2}m_\sigma^2\sigma^2 - \tfrac{1}{3}g_2\sigma^3 - \tfrac{1}{4}g_3\sigma^4 \\ & - \tfrac{1}{4}\Omega^{\mu\nu}\Omega_{\mu\nu} + \tfrac{1}{2}m_\omega^2\omega^\mu\omega_\mu + \tfrac{1}{4}c_3(\omega_\mu\omega^\mu)^2 - \tfrac{1}{4}R^{a\mu\nu}\cdot R^a_{\mu\nu} \\ & + \tfrac{1}{2}m_\rho^2\rho^{a\mu}\cdot\rho^a_\mu - \tfrac{1}{4}F^{\mu\nu}F_{\mu\nu} - e\bar{\Psi}\gamma^\mu A_\mu\tfrac{1}{2}(1-\tau^3)\Psi, \end{aligned} \quad (20)$$

with

$$\Omega^{\mu\nu} = \partial^\mu\omega^\nu - \partial^\nu\omega^\mu, \quad (21)$$

$$R^{a\mu\nu} = \partial^\mu\rho^{a\nu} - \partial^\nu\rho^{a\mu}, \quad (22)$$

$$F^{\mu\nu} = \partial^\mu A^\nu - \partial^\nu A^\mu, \quad (23)$$

where the meson fields are denoted by σ, ω_μ, and ρ_μ^a and their masses are denoted by m_σ, m_ω, and m_ρ, respectively. The nucleon field and rest mass are denoted by Ψ and m. A_μ is the photon field which is responsible for the electromagnetic interaction, $\alpha=1/137$. The effective strengths of the coupling between the mesons and nucleons are, respectively, g_σ, g_ω, and g_ρ. g_2 and g_3 are the nonlinear coupling strengths of the σ meson. c_3 is the self-coupling term of the ω field. The isospin Pauli matrices are written as τ^a, τ^3 being the third component of τ^a.

Under the no-sea approximations and mean-field approximations, the equations of motion for the fields are easily obtained from the variational principle [38–41]:

$$[-i\boldsymbol{\alpha}\cdot\nabla + \beta M^*(\mathbf{r}) + V(\mathbf{r})]\phi_i(\mathbf{r}) = \epsilon_i\phi_i(\mathbf{r}), \quad (24)$$

where the effective mass $M^*(\mathbf{r})=m+g_\sigma\sigma(\mathbf{r})$. The potential $V(\mathbf{r})$ is a timelike component of a Lorentz vector

$$V(\mathbf{r}) = g_\omega\omega_0(\mathbf{r}) + g_\rho\tau^a\rho_0^a(\mathbf{r}) + e[(1-\tau^3)/2]A_0(\mathbf{r}), \quad (25)$$

$$(-\Delta + m_\sigma^2)\sigma(\mathbf{r}) = -g_\sigma\rho_s(\mathbf{r}) - g_2\sigma^2(\mathbf{r}) - g_3\sigma^3(\mathbf{r}), \quad (26)$$

$$(-\Delta + m_\omega^2)\omega_0(\mathbf{r}) = g_\omega\rho_v(\mathbf{r}) - c_3\omega_0^3(\mathbf{r}), \quad (27)$$

$$(-\Delta + m_\rho^2)\rho_0(\mathbf{r}) = g_\rho\rho_3(\mathbf{r}), \quad (28)$$

$$-\Delta A_0(\mathbf{r}) = e\rho_p(\mathbf{r}), \quad (29)$$

where ρ_s, ρ_v, and ρ_p are, respectively, the densities of scalar, baryon, and proton. ρ_3 is the difference between the neutron and proton densities. This set of coupled equations for mesons and nucleons can be solved consistently by iterations. After a final solution is obtained, we can calculate the binding energies, root-mean-square radii of proton, and neutron density distributions, single particle levels. The details of numerical calculations are described in Refs. [38] and [39].

III. NUMERICAL RESULTS AND DISCUSSIONS

We choose three typical sets of force parameters, NL-SH [42], NL3 [43,44], and TM2 [45] for the RMF calculations.

TABLE I. The RMF results with NL-SH and the experimental values. Two binding energies of ^{28}S and ^{12}O are listed where one is the case for the zero effect of neutron pairing and another is the case with the effect of neutron pairing.

	^{32}S	^{28}S	^{16}O	^{12}O
B(expt.)(MeV)	271.78	201.41	127.62	58.53
B(theor.)(MeV)	262.45	201.50(204.46)	128.56	58.60(61.80)
R_c(expt.)(fm)	3.25		2.72	
R_c(theor.)(fm)	3.24	3.29	2.71	2.94
ε(theor.)(MeV)	−5.83	−1.65	−11.55	−1.93

TABLE II. Same as Table I but for the RMF force NL3.

	^{32}S	^{28}S	^{16}O	^{12}O
B (expt.) (MeV)	271.78	201.41	127.62	58.53
B (theor.) (MeV)	265.06	202.37(205.34)	128.74	59.88(63.12)
R_c (expt.) (fm)	3.25		2.72	
R_c (theor.) (fm)	3.23	3.29	2.73	2.98
ϵ (theor.) (MeV)	−7.29	−2.45	−11.45	−2.35

Many calculations show that these parameters can reproduce the ground state properties of nuclei both near the stable line and near the drip line. The experimental isotope shifts of charge root-mean-square radii on some isotopic chains can be quantitatively reproduced by these parameters. We use these parameter sets to calculate the charge density distributions of ^{12,16}O and ^{28,32}S in the RMF model. The pairing gaps for open shell nuclei are included by the Bardeen-Cooper-Schrieffer treatment. The pairing gaps for ^{32}S and ^{16}O are $\Delta_n=\Delta_p=11.2/\sqrt{A}$ MeV and this is a standard input for stable nuclei in nuclear structure calculations. For ^{12}O and ^{28}S, since they are very near the proton-drip line, we assume that the last two protons just occupy the bound levels according to Tanihata [46,47]. For the neutrons in ^{12}O and ^{28}S, we treat them in both cases, with and without neutron pairing force. Different treatments of the neutron pairing force influence the binding energy by a few MeV, while the charge radii and density distributions are almost the same for ^{28}S and ^{12}O. This is because the neutrons are zero charged. In addition, the two nuclei are proton rich and a slight change of the neutron distribution near the Fermi energy does not have much influence on the distribution of the protons.

We list the RMF results of the nuclei ^{32,28}S and ^{12,16}O with the three sets of parameters in Tables I–III, respectively. In these tables, B (MeV), R (fm), and ε (MeV) are, respectively, the binding energy, the root-mean-square (rms) radius of charge distribution, and the single particle energy of the last protons. Two binding energies of ^{28}S and ^{12}O are listed where one is the case for the zero effect of neutron pairing and another is the case with the effect of neutron pairing. The experimental data of the binding energy are taken from the nuclear mass table [48] and those of the rms radius from Ref. [49]. It is seen from Table I that the theoretical binding energy is approximately 1%–6% off. The deviation between the theoretical rms radius and the experimental one is less than 0.02 fm. The single particle energy of the last proton is a small number for ^{12}O and ^{28}S. This reflects the weak binding of the last two protons.

TABLE III. Same as Table I but for the RMF force TM2.

	^{32}S	^{28}S	^{16}O	^{12}O
B (expt.) (MeV)	271.78	201.41	127.62	58.53
B (theor.) (MeV)	265.67	205.46(208.40)	128.69	59.63(62.86)
R_c (expt.) (fm)	3.25		2.72	
R_c (theor.) (fm)	3.32	3.37	2.75	3.03
ε (theor.) (MeV)	−5.52	−1.29	−11.12	−1.24

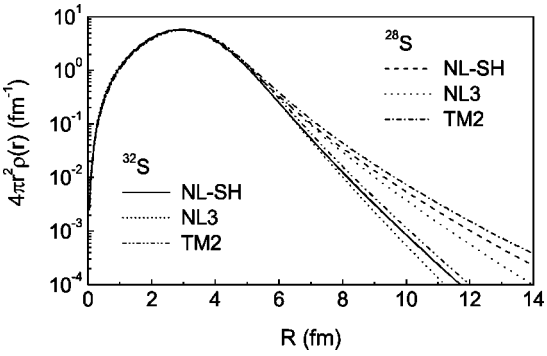

FIG. 1. The charge density distributions of ^{32,28}S calculated with SH-NL, NL3, and TM2 force parameters.

Tables II and III show the RMF results with the NL3 and TM2 parameters. It is seen that the RMF results are also very close to the experimental data. This suggests that the RMF model with NL-SH, NL3, and TM2 parameters approximately reproduces the experimental data of ^{32,28}S and ^{12,16}O. Therefore, it is concluded that the RMF model, without introducing additional adjustments, can be applied to both the stable nuclei ^{16}O and ^{32}S and the unstable nuclei ^{28}S and ^{12}O. As the last two protons in ^{28}S and ^{12}O are weakly bound, their charge distributions could have a much larger spatial extension than those of their stable isotopes. This can be seen clearly from the comparison of the charge density distributions of these nuclei (see Figs. 1 and 2 later).

In Figs. 1 and 2 we plot the charge density distributions of ^{32,28}S and ^{12,16}O. In these figures, the X axis is the radial coordinate and the Y axis is the charge density $4\pi r^2\rho(r)$ $\times$(fm^{-1}). It is seen from Fig. 1 that the charge density distributions of ^{32,28}S with NL-SH parameters are different although the two nuclei have the same proton number. The weak binding of the last two protons in ^{28}S leads to the extended charge density distribution in it. The same conclusion can be drawn from the charge density distributions of ^{32,28}S with NL3 and TM2 parameters. This agrees with the previous theoretical calculations [16,17,29] and with the experimental results [19] of the neighboring nuclei ^{26,27,28}P. The stability of the RMF model for ^{28}S is also approved. For ^{12,16}O, the earlier conclusion holds true. The weak binding of the last two protons in ^{12}O leads to the extended charge density distribution. This can be seen clearly from the charge

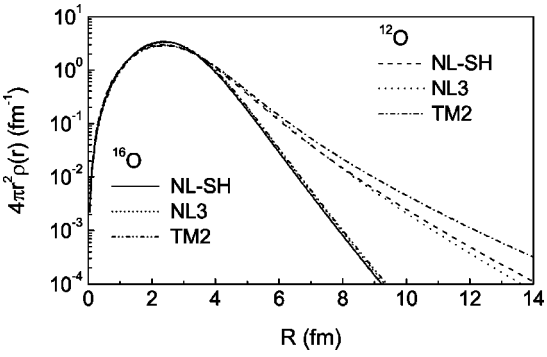

FIG. 2. The charge density distributions of ^{12,16}O calculated with SH-NL, NL3, and TM2 force parameters.

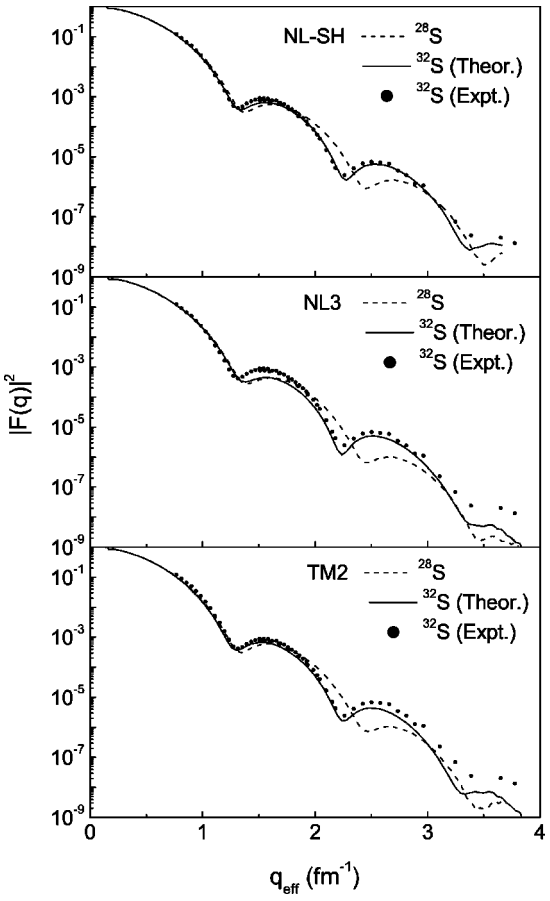

FIG. 3. The variation of the squared form factors of ^{32,28}S with momentum transfer. The theoretical ones are calculated with NL-SH, NL3, and TM2 parameters. The experimental data are taken from Ref. [31].

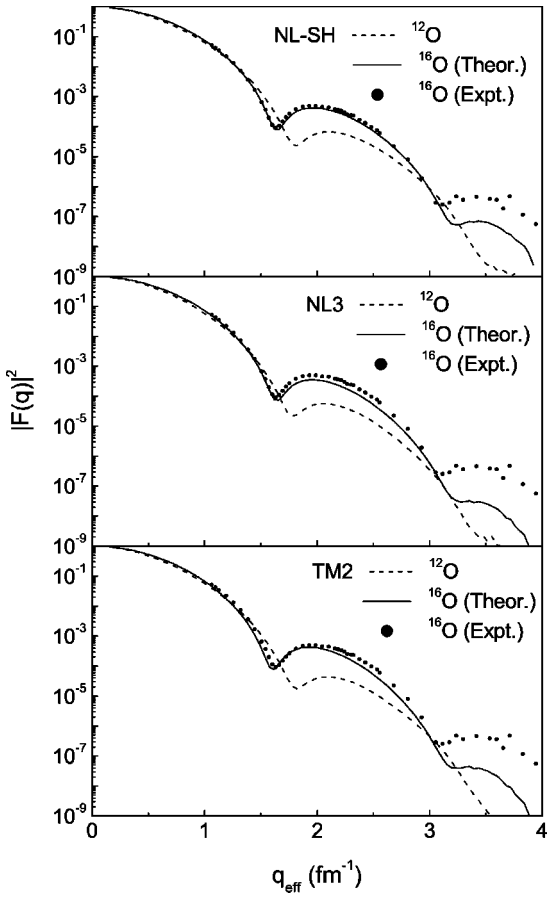

FIG. 4. The variation of the squared form factors of ^{16,12}O with momentum transfer. The theoretical ones are calculated with NL-SH, NL3, and TM2 parameters. The experimental data are taken from Ref. [32].

density distributions shown in Fig. 2. In addition, the two figures display some other information. The slight difference between the charge density distributions of different sets of force parameters shows that the RMF model is not significantly sensitive to the interactions.

In order to find out if the long tail of the charge distribution of the proton-rich nuclei displays observable effects in the process of elastic electron scattering, the elastic form factors and cross sections for the exotic proton-rich nucleus ^{28}S, ^{12}O and their stable isotopes ^{32}S, ^{16}O are calculated in the eikonal approximation. Since the ground state spin and parity of even-even S and O nuclei are 0^+, the elastic scattering cross sections and form factors are determined only by their charge density distributions.

The squared form factors are shown in Figs. 3 and 4, where the input charge distributions are those in Figs. 1 and 2. The top, middle, and bottom part of the two figures correspond to SH-NL, NL3, and TM2 parameters, respectively. The theoretical squared form factors of the stable nuclei ^{32}S and ^{16}O are plotted with solid curves and those of the unstable nuclei ^{28}S and ^{12}O with dashed ones. The experimental cross sections for ^{32}S and ^{16}O have been given by Li *et al.* [31] and Sick *et al.* [32]. The data were taken at two different incident energies for each nucleus in order to cover the range of momentum transfer desired. For the sake of comparison we have here transformed the experimental cross sections into squared form factors. The comparison of our theoretical results for ^{32}S and ^{16}O with the corresponding experimental data, which are denoted with filled circles, is also shown in Figs. 3 and 4.

Before we study the effect of the extended charge distributions of ^{28}S and ^{12}O on the elastic electron scattering, we need to investigate the validity of the combination of the RMF model and the eikonal approximation to the elastic electron-nucleus scattering. For this purpose, we compare the theoretical results with the experimental data for ^{32}S and ^{16}O. It is apparent from Fig. 3 that the theoretical curves (solid) with SH-NL, NL3, and TM2 parameters and the experimental ones (filled circles) for ^{32}S almost coincide in the range of low and moderate-momentum transfer ($q \leqslant 3$ fm^{-1}). Theoretical results have a very good agreement with the experimental data in this range of momentum transfer. At high-momentum transfers, a deviation occurs between the theoretical form factor and the experimental one. Since the form factor in this range of momentum transfer is mainly sensitive to the details of the inner part of the charge density distribution [32], its occurrence indicates that the theoretical charge density distribution has a departure from the experimental one around the center of the nucleus. This means that the RMF model can reproduce the charge density distribution

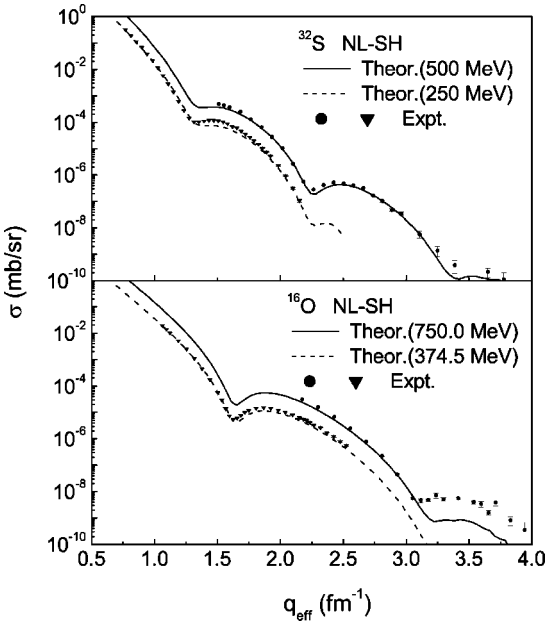

FIG. 5. The comparison of the experimental cross sections of ^{32}S and ^{16}O with the theoretical ones which are calculated with NL-SH parameters.

for ^{32}S very well except near the center of the nucleus. It is concluded that the combination of the RMF model with the eikonal approximation, without introducing additional adjustments, can approximately reproduce the experimental data of elastic electron scattering on the stable nucleus ^{32}S. The comparison of the theoretical results with the experimental ones for ^{16}O arrives at the same conclusion (see Fig. 4). In Fig. 5 we also give the comparison of the calculated cross sections (NL-SH parameters) with the experimental ones for ^{32}S and ^{16}O. It shows a very good agreement of the theoretical results with the experimental data. The cross sections of the other two sets of force parameters also agree well with the experimental ones (the figures are not given). Hence, the stability and validity of the combination of the RMF model with the eikonal approximation to the elastic electron-nucleus scattering from the stable isotopes of S and O are approved.

Under the precondition of the validity of the combination of the RMF model with the eikonal approximation to the elastic electron-nucleus scattering from the stable isotopes of S and O, we now discuss the form factors of the unstable nuclei ^{28}S and ^{12}O. It can be seen from Fig. 3 that although the trend of the form factors of the unstable nucleus ^{28}S is similar to that of its stable isotope ^{32}S, there appear to be two important differences, both apparent in Fig. 3. First, the position of the minimums of ^{28}S has a large outward shift as compared with that of ^{32}S. The outward shift of the first, the second, and the third minimum are approximately, 0.03, 0.183, and 0.118 fm^{-1}, respectively. These shifts, except 0.03 fm^{-1}, can be precisely measured with the current elastic electron-nucleus scattering experiments. Second, the amplitude has a significant deviation. For a specific momentum transfer $q=2.65$ fm^{-1}, the amplitude deviation of the form factors of ^{32}S and ^{28}S is about $\Delta|F(q)|^2 \simeq 0.5\times10^{-5}$. This deviation can also be observed with elastic electron-nucleus experiments. These imply that the differences between the form factor of ^{28}S and that of ^{32}S have observable effects.

The earlier analysis holds true for the differences between the form factor of ^{16}O and that of ^{12}O (see Fig. 4). The outward shift of the first and the second minimum are approximately 0.17 and 0.35 fm^{-1}, the amplitude deviation at the momentum transfer $q=2.30$ fm^{-1} is about $\Delta|F(q)|^2 \simeq 1.46\times10^{-4}$. These differences also bring observable effects in elastic electron-nucleus scattering experiments.

It is known that the elastic electron scattering form factor of a nucleus is directly related to its charge density distribution. Therefore, the difference between the form factor of ^{28}S and that of ^{32}S is due to the different charge density distributions of the two nuclei. Since the difference of charge density distribution between ^{28}S and ^{32}S is mainly caused by the difference of the charge density distribution of the last two protons in ^{28}S and ^{32}S, we conclude that the difference between the form factor of ^{28}S and that of ^{32}S indicates the difference in the density distribution of the last two protons in the two nuclei. For the nuclei ^{16}O and ^{12}O, we can draw the same conclusion by similar argument. This implies that the effect of the change of the density distribution of the last two protons on the charge density distribution of S and O can be observed in elastic electron-nucleus scattering experiments by comparing the form factors of ^{28}S and ^{32}S and of ^{12}O and ^{16}O.

In order to search the influence of the long tail of the charge distributions of ^{28}S and ^{12}O on elastic electron-nucleus scattering, we need to further find out which part of the form factor is sensitive to the tail of the charge density distribution. It is known from the fitting to the experimental data of ^{32}S [31] that the form factors in the range of moderate-momentum transfer 1 fm$^{-1}\leqslant q\leqslant 2.8$ fm^{-1} are not sensitive to the modification of charge density around the center of nucleus. The form factors in the range of $q>2.8$ fm^{-1} are sensitive to the variation of charge density near the center of nucleus [31]. Thus, the position of the third minimum is sensitive to the charge density distribution around the center of nucleus, while those of the first and the second minima are insensitive to the charge density distribution around the center of nucleus [31].

For ^{16}O there are similar conclusions [32]. The form factors in the range of $q\leqslant 2.8$ fm^{-1} are not sensitive to the variation of charge density around the center of nucleus. The form factors in the range of $q>2.8$ fm^{-1} are sensitive to the variation of the charge density near the center of nucleus [32]. The position of the second minimum of the form factor of ^{16}O is also sensitive to the inner part of the charge distribution, while that of the first minimum is insensitive to the inner part of the charge distribution [32].

Now we discuss the influence of the tail of the charge density distribution on the form factor. It is known from the fitting to the experimental data of ^{12}C [32] that the form factors in the range of moderate-momentum transfer (1 fm$^{-1}\leqslant q\leqslant 3$ fm^{-1}) is sensitive to the change of the tail part of the charge density [32], while those at high-momentum transfers to the change of the inner part of the charge distribution [32]. It is expected that the conclusions of ^{12}C work also for O and S isotopes.

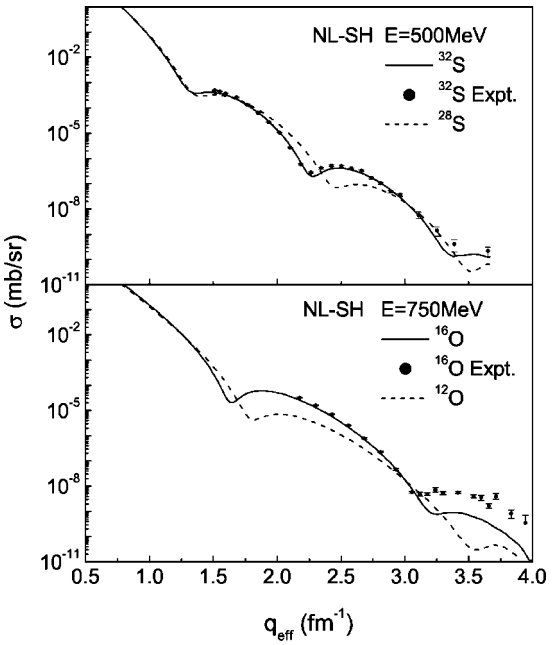

FIG. 6. The variation of the cross sections of ^{28,32}S and ^{12,16}O with momentum transfer, which are calculated with NL-SH parameters.

From the earlier discussions it is now clear that the form factors of a nucleus at moderate-momentum transfers, approximately 1 fm$^{-1} \leqslant q \leqslant 3$ fm^{-1}, are sensitive to the tail of the charge distribution, while those at high momentum transfers are mainly affected by the inner part of the charge distribution. Thus, we may consider the differences of the form factors at moderate-momentum transfers between ^{28}S and ^{32}S and between ^{12}O and ^{16}O as the influence of the long tails in ^{28}S and ^{12}O. This suggests that the spatial extension of the charge distributions in ^{28}S and ^{12}O can be observed in elastic electron scattering experiments. In addition, for a given nucleus, the form factor differences at high-momentum transfers between different sets of parameters can be explained as follows. Since the form factors at high-momentum transfers are sensitive to the inner part of the charge distribution, we consider that with different sets of parameters the RMF theory gives a slightly different prediction for the charge distribution near the center of nucleus.

Figure 6 displays the theoretical cross sections of ^{28,32}S and ^{12,16}O with NL-SH parameters. They exhibit the same behavior as that of the form factors in Figs. 3 and 4. In the same way that we analyze the form factors, we deduce that, for S and O, the cross sections in the range of moderate-momentum transfer are very sensitive to the changes of the charge density distributions of the last two protons. In order to show the observable effects brought by the the changes of the charge density distributions of the last two protons, we also plot the experimental cross sections and error bars of ^{32}S and ^{16}O in Fig. 6 [31,32]. It is seen that the error bars are very small in the range of moderate-momentum transfer. So the cross sections can be very accurately measured in this range of momentum transfer. While, compared with the error bars, the cross section differences, $|\sigma(^{28}\mathrm{S})\text{-}\sigma(^{32}\mathrm{S})|$ and $|\sigma(^{12}\mathrm{O})\text{-}\sigma(^{16}\mathrm{O})|$, are much larger. This indicates that the cross section difference has observable effect and can be measured in electron-nucleus scattering experiments. As the cross sections with the other two sets of parameters (NL3 and TM2) are very similar to those with NL-SH, we do not discuss them here.

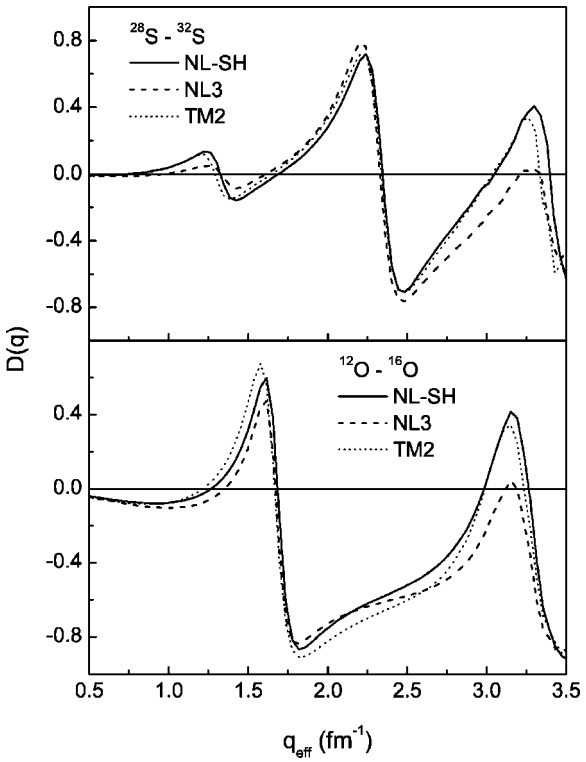

FIG. 7. The cross section differences $D(q)$ for ^{28}S and ^{32}S and for ^{12}O and ^{16}O, which are calculated with the three sets of force parameters NL-SH, NL3, and TM2.

Figure 7 shows the difference of the cross section $D(q)$ which is defined as

$$D(q) = \frac{\sigma_{28}(q) - \sigma_{32}(q)}{\sigma_{28}(q) + \sigma_{32}(q)} \tag{30}$$

for S and

$$D(q) = \frac{\sigma_{12}(q) - \sigma_{16}(q)}{\sigma_{12}(q) + \sigma_{16}(q)} \tag{31}$$

for O. This figure gives a clearer presentation of the minimum shifts and the amplitude differences. The sensitivity of the cross section of S and O to the variation of the charge density distribution of the last two protons is evidently displayed.

From the earlier discussion we may conclude that the form factors and cross sections of S and O in the range of moderate-momentum transfer are sensitive to the existence of the long tail of the charge distribution. Both the minimum shifts and the amplitude deviations of the form factors of ^{28}S and ^{12}O (compared with those of ^{32}S and ^{16}O) have observable effects. These effects show that elastic electron-nucleus scattering could be used as an effective tool to study the

proton drip-line nuclei. Thus it will be very interesting to observe experimentally these effects (part of the MUSES project at RIKEN [24]).

Until now, we have discussed the effect of the extended charge density distribution of a proton drip-line nucleus on elastic electron scattering. Cross sections on stable targets can be measured with great accuracy. While this will not be the case for the future beam-beam experiments. The experimental situation for electron scattering from unstable nuclei is not as clear as that from stable ones. The measurement of the cross sections on unstable nuclei will be more difficult and the experimental accuracy is unknown. However, studies of electron scattering on exotic proton drip-line nuclei will be possible at the double storage ring MUSES at RIKEN [24]. So we conclude that, when it become possible to measure the cross sections of electron scattering on exotic proton drip-line nuclei, the effect of the extended charge density distribution on elastic electron scattering may be observed.

Finally, it is interesting to have a brief discussion of the dependence of our result on the RMF force parameters. It is seen from Figs. 2 and 3 that the result from each set of parameters agrees well with the experimental data in the range of low and moderate-momentum transfer for the stable nuclei ^{32}S and ^{16}O. For the proton drip-line nuclei ^{28}S and ^{12}O, the results of the three different sets of parameters are also very close to each other. A more detailed display of the coincidence of the results of the three sets of parameters for ^{28}S and ^{12}O is shown in Fig. 7. One can see from Fig. 7 that the values of the cross sections and the positions of the cross section minimums calculated with the three sets of parameters are approximately equal in the range of low and moderate-momentum transfer. These imply that the calculated results are not significantly sensitive to the force parameters and consequently our conclusion drawn from them is reliable.

IV. CONCLUSION

In summary we have combined the RMF model with the eikonal approximation for the elastic electron scattering from the stable nuclei ^{32}S, ^{16}O and the exotic proton-rich isotopes ^{28}S, ^{12}O. The elastic electron scattering cross sections and squared form factors of ^{32}S, ^{16}O and ^{28}S, ^{12}O are calculated and compared, where the three sets of force parameters NL-SH, NL3, and TM2 have been used. The effects of the long tail of the charge distribution on the form factors and cross sections of S and O are analyzed. It is found that there is a significant difference between the squared form factors or the cross sections of the exotic proton drip-line nuclei and those of the stable nuclei in the range of the moderate-momentum transfer. We attribute this significant difference to the influence of the charge density distribution of the last two protons in ^{28}S and ^{12}O. Since the difference of the form factors between a stable nucleus and its proton drip-line isotope has observable effects, we consider that elastic electron scattering is an effective tool to investigate proton-halo phenomena of proton-rich nuclei. Another result of this paper is that our calculations and analyses provide a new testing ground of the reliability and stability for the RMF, especially on the nuclear wave functions for the exotic proton-rich nuclei. We expect that the experiments of elastic electron-nucleus scattering on unstable nuclei will soon be available at the electron-nucleus collider which is being built at RIKEN in Japan [24].

ACKNOWLEDGMENTS

Z.R. thanks Professor W. Q. Shen, Professor H. Q. Zhang, and Professor Z. Y. Ma for discussions on electron scattering. This work is supported by the National Natural Science Foundation of China (Grant No. 10125521), by the 973 National Major State Basic Research and Development of China (Grant No. G2000077400), by the CAS Knowledge Innovation Project No. KJCX2-SW-N02, and by the Research Fund of Higher Education under Contract No. 20010284036.

[1] I. Tanihata, H. Hamagaki, O. Hashimoto, Y. Shida, N. Yoshikawa, K. Sugimoto, O. Yamakawa, T. Kobayashi, and N. Takahashi, Phys. Rev. Lett. **55**, 2676 (1985).

[2] I. Tanihata, T. Kobayashi, O. Yamakawa, S. Shimoura, K. Ekuni, K. Sugimoto, N. Takahashi, and T. Shimoda, Phys. Lett. B **206**, 592 (1988).

[3] W. Mittig, J. M. Chouvel, Z. W. Long, L. Bianchi, A. Cunsolo, B. Fernandez, A. Foti, J. Gastebois, A. Gillibert, C. Gregoire, Y. Schutz, and C. Stephan, Phys. Rev. Lett. **59**, 1889 (1987).

[4] T. Kobayashi, O. Yamakawa, K. Omata, K. Sugimoto, T. Shimoda, N. Takahashi, and I. Tanihata, Phys. Rev. Lett. **60**, 2599 (1988).

[5] M. G. Saint-Laurent, R. Anne, D. Bazin, D. Guillemaud-Mueller, U. Jahnke, J. G. Ming, A. C. Mueller, J. F. Bruandet, F. Glasser, S. Kox, E. Liatard, Tsan Ung Chan, G. J. Costa, C. Heitz, Y. El-Masri, F. Hanappe, R. Bimbot, E. Arnold, and R. Neugart, Z. Phys. A **332**, 457 (1989).

[6] T. Nilsson, F. Humbert, W. Schwab, H. Simon, M. H. Smedberg, M. Zinser, Th. Blaich, M. J. G. Borge, L. V. Chulkov, Th. W. Elze, H. Emling, H. Geissel, K. Grimm, D. Guillemaud-Mueller, P. G. Hansen, R. Holzmann, H. Irnich, B. Jonson, J. G. Keller, H. Klingler, A. A. Korsheninnikov, J. V. Kratz, R. Kulessa, D. Lambrecht, Y. Leifels, A. Magel, M. Mohar, A. C. Mueller, G. Münzenberg, F. Nickel, G. Nyman, A. Richter, K. Riisager, C. Scheidengerger, G. Schrieder, B. M. Sherrill, K. Stelzer, J. Stroth, O. Tengblad, W. Trautmann, E. Wajda, M. V. Zhukov, and E. Zude, Nucl. Phys. **A598**, 418 (1996).

[7] M. Zinser, F. Humbert, T. Nilsson, W. Schwab, Th. Blaich, M. J. G. Borge, L. V. Chulkov, H. Eickhoff, Th. W. Elze, H. Emling, B. Franzke, H. Freiesleben, H. Geissel, K. Grimm, D. Guillemaud-Mueller, P. G. Hansen, R. Holzmann, H. Irnich, B. Jonson, J. G. Keller, O. Klepper, H. Klingler, J. V. Kratz, R. Kulessa, D. Lambrecht, Y. Leifels, A. Magel, M. Mohar, A. C.

Mueller, G. Münzenberg, F. Nickel, G. Nyman, A. Richter, K. Riisager, C. Scheidengerger, G. Schrieder, B. M. Sherrill, H. Simon, K. Stelzer, J. Stroth, O. Tengblad, W. Trautmann, E. Wajda, and E. Zude, Phys. Rev. Lett. **75**, 1719 (1995).

[8] N. A. Orr, N. Anantaraman, Sam M. Austin, C. A. Bertulani, K. Hanold, J. H. Kelley, D. J. Morrissey, B. M. Sherrill, G. A. Souliotis, M. Thoennessen, J. S. Winfield, and J. A. Winger, Phys. Rev. Lett. **69**, 2050 (1992).

[9] R. Anne, S. E. Arnell, R. Bimbot, H. Emling, D. Guillemaud-Mueller, P. G. Hansen, L. Johannsen, B. Jonson, M. Lewitowicz, S. Mattsson, A. C. Mueller, R. Neugart, G. Nyman, F. Pougheon, A. Richter, K. Riisager, M. G. Saint-Laurent, G. Schrieder, O. Sorlin, and K. Wilhelmsen, Phys. Lett. B **250**, 19 (1990).

[10] Z. Ren and G. Xu, Phys. Lett. B **252**, 311 (1990).

[11] G. F. Bertsch and H. Esbensen, Ann. Phys. (N.Y.) **209**, 327 (1991).

[12] M. V. Zhukov, B. V. Danilin, D. V. Fedorov, J. M. Bang, I. J. Thompson, and J. S. Vaagen, Phys. Rep. **231**, 151 (1993).

[13] P. G. Hansen, A. S. Jensen, and B. Jonson, Annu. Rev. Nucl. Part. Sci. **45**, 591 (1995).

[14] J. S. Al-khalili, J. A. Tostevin, and I. J. Thompson, Phys. Rev. C **54**, 1843 (1996).

[15] T. Otsuka, N. Fukunishi, and H. Sagawa, Phys. Rev. Lett. **70**, 1385 (1993).

[16] Z. Ren, B. Chen, Z. Ma, and G. Xu, Phys. Rev. C **53**, R572 (1996).

[17] B. A. Brown and P. G. Hansen, Phys. Lett. B **381**, 391 (1996).

[18] A. Navin, D. Bazin, B. A. Brown, B. Davids, G. Gervais, T. Glasmacher, K. Govaert, P. G. Hansen, M. Hellström, R. W. Ibbotson, V. Maddalena, B. Pritychenko, H. Scheit, B. M. Sherrill, M. Steiner, J. A. Tostevin, and J. Yurkon, Phys. Rev. Lett. **81**, 5089 (1998).

[19] H. Y. Zhang, W. Q. Shen, Z. Z. Ren, Y. G. Ma, W. Z. Jiang, Z. Y. Zhu, X. Z. Cai, D. Q. Fang, C. Zhong, L. P. Yu, Y. B. Wei, W. L. Zhu, Z. Y. Guo, G. Q. Xiao, J. S. Wang, J. C. Wang, Q. J. Wang, J. X. Li, M. Wang, and Z. Q. Chen, Nucl. Phys. **A707**, 303 (2002).

[20] R. Morlock, R. Kunz, A. Mayer, M. Jaeger, A. Mueller, J. W. Hammer, P. Mohr, H. Oberhummer, G. Staudt, and V. Koelle, Phys. Rev. Lett. **79**, 3837 (1997).

[21] M. V. Zhukov and I. J. Thompson, Phys. Rev. C **52**, 3505 (1995).

[22] Z. Li, W. Liu, X. Bai, Y. Wang, G. Lian, Z. Li, and S. Zeng, Phys. Lett. B **527**, 50 (2002).

[23] H. Y. Zhang, W. Q. Shen, Y. G. Ma, X. Z. Cai, D. Q. Fang, C. Zhong, Y. B. Wei, J. G. Chen, X. F. Zhou, G. L. Ma, K. Wang, Z. Z. Ren, W. L. Zhan, Z. Y. Guo, G. Q. Xiao, H. S. Xu, J. S. Wang, Z. Y. Sun, J. X. Li, M. Wang, Z. Q. Chen, Z. G. Xiao, W. F. Li, J. F. Li, Z. G. Hu, J. Bai, and L. X. Chen, Mod. Phys. Lett. A **18**, 151 (2003).

[24] T. Suda, K. Maruyama, and I. Tanihata, RIKEN Accel. Prog. Rep. **34**, 49 (2001).

[25] An international accelerator facility for beams of ions and antiprotons, GSI report, 2002.

[26] Y. K. Gambhir, P. Ring, and A. Thimet, Ann. Phys. (N.Y.) **198**, 132 (1990).

[27] C. J. Horowitz and B. D. Serot, Nucl. Phys. **A368**, 503 (1981).

[28] Z. Ma, H. Shi, and B. Chen, Phys. Rev. C **50**, 3170 (1994).

[29] Z. Ren, W. Mittig, and F. Sarazin, Nucl. Phys. **A652**, 250 (1999).

[30] Z. Ren, W. Mittig, B. Chen, and Z. Ma, Phys. Rev. C **52**, R20 (1995).

[31] G. C. Li, M. R. Yearian, and I. Sick, Phys. Rev. C **9**, 1861 (1974).

[32] I. Sick and J. S. McCarthy, Nucl. Phys. **A150**, 631 (1970).

[33] S. J. Wallace, Ann. Phys. (N.Y.) **78**, 190 (1973).

[34] S. J. Wallace, Phys. Rev. D **9**, 406 (1974).

[35] R. G. Newton, *Scattering Theory of Waves and Particles* (McGraw-Hill, New York, 1966).

[36] A. Baker, Phys. Rev. **134**, B240 (1964).

[37] R. J. Glauber, *Lectures in Theoretical Physics* (Interscience, New York, 1959), Vol. I.

[38] P. Ring, Prog. Part. Nucl. Phys. **37**, 139 (1996).

[39] L. S. Warrier and Y. K. Gambhir, Phys. Rev. C **49**, 871 (1994).

[40] I. Tanihata, D. Hirata, T. Kobayashi, S. Shimoura, K. Sugimoto, and H. Toki, Phys. Lett. B **289**, 261 (1992).

[41] D. Hirata, H. Toki, I. Tanihata, and P. Ring, Phys. Lett. B **314**, 168 (1993).

[42] M. M. Sharma, M. A. Nagarajian, and P. Ring, Phys. Lett. B **312**, 377 (1993).

[43] G. A. Lalazissis, J. Konig, and P. Ring, Phys. Rev. C **55**, 540 (1997).

[44] Z. Patyk, A. Baran, J. F. Berger, J. Decharge, J. Dobaczewski, P. Ring, and A. Sobiczewski, Phys. Rev. C **59**, 704 (1999).

[45] Y. Sugahara and H. Toki, Nucl. Phys. **A579**, 557 (1994).

[46] I. Tanihata, D. Hirata, and H. Toki, Nucl. Phys. **A583**, 769 (1995).

[47] A. Ozawa, T. Kobayashi, T. Suzuki, K. Yoshida, and I. Tanihata, Phys. Rev. Lett. **84**, 5493 (2000).

[48] G. Audi and A. H. Wapstra, Nucl. Phys. **A565**, 1 (1993).

[49] H. De Vries, C. W. De Jager, and C. De Vries, At. Data Nucl. Data Tables **36**, 496 (1987).